

Hyperspherical Analysis of Dimer-Dimer Scattering in One-Dimensional Systems

Jia Wang^{1*}, Hui Hu² and Xia-Ji Liu³

¹Centre for Quantum Technology Theory, Swinburne University of Technology, Melbourne, 3122, Australia.

*Corresponding author(s). E-mail(s): jiawanghome@gmail.com;

Abstract

We present a comprehensive analysis of four-body scattering in one-dimensional (1D) quantum systems using the adiabatic hyperspherical representation (AHR). Focusing on dimer-dimer collisions between two species of fermions interacting via the sinh-cosh potential, we implement the slow variable discretization (SVD) method to overcome numerical challenges posed by sharp avoided crossings in the potential curves. Our numerical approach is benchmarked against exact analytical results available in integrable regimes, demonstrating excellent agreement. We further explore non-integrable regimes where no analytical solutions exist, revealing novel features such as resonant enhancement of the scattering length associated with tetramer formation. These results highlight the power and flexibility of the AHR+SVD framework for accurate few-body scattering calculations in low-dimensional quantum systems, and establish a foundation for future investigations of universal few-body physics in ultracold gases.

1 Introduction

Since the groundbreaking development of laser cooling and trapping of atoms [1], the field of ultracold quantum gases has rapidly expanded and made a profound impact on the study of fundamental quantum phenomena [2–4]. At temperatures as low as a billionth of a degree Kelvin (nano-Kelvin, nK) and densities ranging from 10^{12} to 10^{15} cm^{-3} , these systems reach the quantum degenerate regime, where the atomic de Broglie wavelength exceeds the typical interparticle spacing [5, 6]. A variety of trapping techniques enable the realization of low-dimensional systems, while Feshbach resonances allow for precise and tunable control over interparticle interactions [7, 8].

This extraordinary level of control, combined with recent advances in theoretical and computational techniques, makes ultracold gases an ideal platform for exploring few-body quantum physics and performing quantitative comparisons between theory and experiment.

One of the most striking few-body phenomena predicted in this context is the Efimov effect. In the early 1970s, Vitaly Efimov predicted that three identical resonant bosons can form a series of three-body bound states—now known as Efimov trimers—characterized by a discrete scaling symmetry [9]. Remarkably, the scaling factor is independent of short-range interaction details, making the phenomenon universal. Once considered purely theoretical, Efimov states have since been observed in numerous ultracold gas experiments [10–20]. Moreover, new forms of universality have emerged in these systems, with Efimov trimers displaying properties that reflect the long-range van der Waals tails of the underlying two-body potentials [21–25]. Other exotic few-body states, including super-Efimov [26–28] and semi-super Efimov states [29], have been theoretically proposed and are being actively explored in ultracold gases, particularly in systems with tunable dimensionality.

In this work, we investigate the four-body scattering problem in one-dimensional (1D) systems. A system of four fermions—two in one component and two in another—is the simplest nontrivial few-body configuration that captures the essential physics of ultracold fermionic gases. We numerically obtain essentially exact solutions to this problem using the adiabatic hyperspherical representation (AHR). AHR is a well-established method in atomic, molecular, and optical physics, as well as in nuclear and condensed matter contexts. It has been particularly successful in describing few-body scattering in ultracold gases, notably in the seminal work by Greene and collaborators on ultracold collisions [30–36] and Efimov physics [23, 37, 38]. While AHR can also be applied to four-body problems in three dimensions, doing so typically requires carefully tailored variational basis sets due to the increased number of degrees of freedom [39–41].

In contrast, the reduced dimensionality of 1D systems offers computational advantages, allowing us to apply numerically exact diagonalization methods using simple B-spline basis functions. Although some adiabatic hyperspherical potential curves for 1D four-body systems have been presented in previous studies [39], scattering observables such as the dimer-dimer scattering length have not yet been computed. A key challenge in these calculations is the presence of sharp avoided crossings in the adiabatic potential curves, which complicate numerical integration of the coupled channel equations.

To overcome this difficulty, we employ the slow variable discretization (SVD) method, which enables stable and accurate computation of scattering observables [42, 43]. In particular, we focus on a model interaction known as the sinh-cosh potential, for which analytical solutions are available for certain parameter regimes [44]. We benchmark our numerical results against these exact solutions, and further extend the analysis to parameter ranges where no analytical solutions exist.

2 Theory

2.1 Hyperspherical Coordinate

We consider four particles confined to one dimension (1D), with coordinates r_j and masses m_j (for $j = 1, 2, 3, 4$). It is convenient to begin by transforming to ‘‘H’’-type Jacobi coordinates, where the configuration is illustrated in Fig. 1 (a). We define

$$\begin{aligned}
 y_1 &= \sqrt{\frac{\mu_1}{\mu_{4b}}} x_1 = \sqrt{\frac{\mu_1}{\mu_{4b}}} (r_1 - r_2), \\
 y_2 &= \sqrt{\frac{\mu_2}{\mu_{4b}}} x_2 = \sqrt{\frac{\mu_2}{\mu_{4b}}} (r_3 - r_4), \\
 y_3 &= \sqrt{\frac{\mu_3}{\mu_{4b}}} x_3 = \sqrt{\frac{\mu_3}{\mu_{4b}}} \left(\frac{r_1 + r_2}{2} - \frac{r_3 + r_4}{2} \right), \\
 y_4 &= x_4 = \frac{r_1 + r_2 + r_3 + r_4}{4}.
 \end{aligned} \tag{1}$$

Here, x_i are the conventional Jacobi coordinate, while y_i are their corresponding mass-scaled forms. The centre-of-mass coordinate $y_4 = x_4$ can usually be separated from the dynamics. The reduced masses are defined by $\mu_1^{-1} = m_1^{-1} + m_2^{-1}$, $\mu_2^{-1} = m_3^{-1} + m_4^{-1}$, and $\mu_3^{-1} = (m_1 + m_2)^{-1} + (m_3 + m_4)^{-1}$. The four-body reduced mass μ_{4b} can essentially be defined arbitrarily as long as the relative kinetic energy operator are defined consistently. We choose $\mu_{4b} = \sqrt[3]{\Pi_j m_j / (2 \sum_j m_j)}$, and the relative kinetic energy operator reads as

$$\hat{T} = - \sum_{i=1}^3 \frac{\hbar^2}{2\mu_i} \frac{\partial^2}{\partial x_i^2} = - \frac{\hbar^2}{2\mu_{4b}} \sum_{i=1}^3 \frac{\partial^2}{\partial y_i^2}. \tag{2}$$

Hereafter, we focus on the equal-mass case: of $m_j = m$ for all j . Then $\mu_{4b} = m/2$, $\mu_1 = m/2$, $\mu_2 = m/2$, and $\mu_3 = m$. We assume particles 1 and 2 are identical fermions, as are particles 3 and 4, but the two pairs are distinguishable from each other. The pairwise distances r_{ij} between the particles i and j become:

$$\begin{aligned}
 r_{12} &= y_1, \\
 r_{13} &= y_1/2 - y_2/2 + y_3/\sqrt{2}, \\
 r_{14} &= y_1/2 + y_2/2 + y_3\sqrt{2}, \\
 r_{23} &= -y_1/2 - y_2/2 + y_3/\sqrt{2}, \\
 r_{24} &= -y_1/2 + y_2/2 + y_3/\sqrt{2}, \\
 r_{34} &= y_2.
 \end{aligned} \tag{3}$$

We introduce hyperspherical coordinates in analogy with three-dimensional (3D) spherical coordinate:

$$\begin{aligned} y_1 &= R \sin \phi \sin \theta \\ y_2 &= R \cos \phi \sin \theta \\ y_3 &= R \cos \theta \end{aligned} \quad (4)$$

with the hyperradius $R \in [0, \infty)$, and the hyperangles $\Omega \equiv \{\theta, \phi\}$ where $\phi \in [0, 2\pi)$ and $\theta \in [0, \pi]$. Figure 1 (b) illustrates the mapping between the geometric configuration of the four particles and the hyperangles. For clarity, we only show the region $\phi \in [0, \pi/2]$ and $\theta \in [0, \pi]$, as the full configuration space can be reconstructed using symmetry operations (see discussion below).

The relative kinetic energy operator becomes:

$$\hat{T} = -\frac{\hbar^2}{2\mu_{4b}} \frac{1}{R} \frac{\partial^2}{\partial R^2} R + \frac{\hat{L}(\Omega)^2}{2\mu_{4b}R^2}, \quad (5)$$

with the hyperangular momentum operator defined as:

$$\hat{L}(\Omega)^2 = -\hbar^2 \left[\frac{1}{\sin \theta} \frac{\partial}{\partial \theta} \sin \theta \frac{\partial}{\partial \theta} + \frac{1}{\sin^2 \theta} \frac{\partial^2}{\partial \phi^2} \right]. \quad (6)$$

This operator has the same form as the angular momentum operator in three-dimensional space, which is expected since the number of relative degrees of freedom in our four-body problem is also three.

The four-body Schrödinger equation (after separating the center-of-mass degree of freedom) is given by

$$\left[-\frac{\hbar^2}{2\mu_{4b}} \frac{1}{R} \frac{\partial^2}{\partial R^2} R + \frac{\hat{L}(\Omega)^2}{2\mu_{4b}R^2} + V(R, \Omega) \right] \Psi(R, \Omega) = E\Psi(R, \Omega). \quad (7)$$

We define a rescaled wave function $\psi = R\Psi$, which satisfies

$$\left[-\frac{\hbar^2}{2\mu_{4b}} \frac{\partial^2}{\partial R^2} + \frac{\hat{L}(\Omega)^2}{2\mu_{4b}R^2} + V(R, \Omega) \right] \psi(R, \Omega) = E\psi(R, \Omega), \quad (8)$$

where $V(R, \Omega)$ denotes the interaction potential among particles.

2.2 The sinh-cosh potential

For ultracold atomic systems, the total interaction potential can usually be modeled as a sum of pairwise interactions:

$$V(R, \Omega) = \sum_{i < j} v_{ij}(r_{ij}), \quad (9)$$

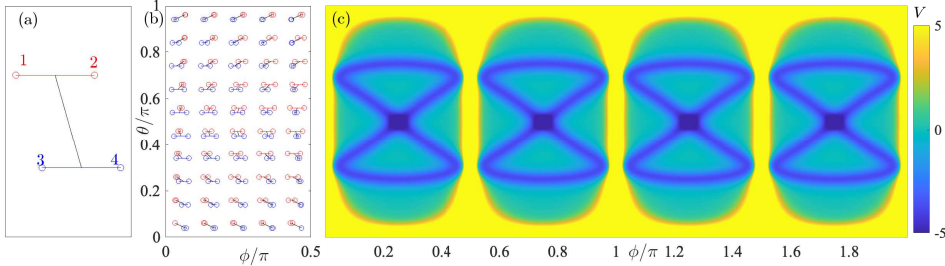


Fig. 1 (a) Schematic illustration of the four-particle configuration. As the system is one-dimensional, only the horizontal displacement is physically meaningful; vertical offsets are used solely for visual clarity. (b) Mapping between the geometric configuration of particles and the hyperangular coordinates θ and ϕ . (c) The four-body potential $V(R, \Omega)$ plotted as a function of angles at fixed hyperradius $R = 10$. The pairwise two-body interaction is modeled using the sinh-cosh potential with parameters $s = s' = 1.5$.

where the interparticle distances r_{ij} can then be explicitly written in terms of hyperspherical coordinates:

$$\begin{aligned}
 r_{12} &= R \sin \phi \sin \theta, \\
 r_{13} &= R [\sin \theta \sin (\phi - \pi/4) + \cos \theta] / \sqrt{2}, \\
 r_{14} &= R [\sin \theta \sin (\phi + \pi/4) + \cos \theta] / \sqrt{2}, \\
 r_{23} &= -R [\sin \theta \sin (\phi + \pi/4) - \cos \theta] / \sqrt{2}, \\
 r_{24} &= -R [\sin \theta \sin (\phi - \pi/4) - \cos \theta] / \sqrt{2}, \\
 r_{34} &= R \cos \phi \sin \theta.
 \end{aligned} \tag{10}$$

The system we now wish to focus consists of two kinds of fermions with the same mass m , distinguished only by a label $\sigma = \pm 1$. The pair-wise potential considered here are called the sinh-cosh potential [44], which follows the form of

$$v_{\sigma_i \sigma_j}(r_{ij}) = \frac{s'(s'+1)}{\sinh^2(r_{ij}/r_c)} \left(\frac{1 + \sigma_i \sigma_j}{2} \right) - \frac{s(s+1)}{\cosh^2(r_{ij}/r_c)} \left(\frac{1 - \sigma_i \sigma_j}{2} \right), \tag{11}$$

where $s', s > 0$. This form ensures that like particles (same σ) interact repulsively, while unlike particles experience an attractive interaction. In this sense, the system is analogous to an electron-hole model, where σ can be interpreted as an effective charge. At large distances, both types of interactions decay exponentially with a characteristic length scale r_c , which we hereafter set to unity. The corresponding natural energy scale is then $E_c = \hbar^2/mr_c^2$. Throughout this work, we adopt r_c and E_c as natural units to interpret the length and energy scales in the figures.

Figure 1 (c) shows the four-body potential at hyperradius $R = 10$ as a function of the hyperangles. The plot reveals a clear fourfold symmetry, with identical potential landscapes across four regions. Notably, a deep minimum appears near $(\theta, \phi) = (\pi/2, \pi/4)$, indicated by the dark blue region, while a lighter blue figure-eight-shaped stripe and a broader light green plateau surround it. As we will see,

these regions correspond to different physical configurations: the deep minimum supports dimer-dimer scattering states, the lighter stripe indicates dimer-atom-atom configurations, and the outer plateau corresponds to four free atoms.

One interesting property of the sinh-cosh potential is that the two-body scattering properties are known analytically [44]. For the repulsive sinh-potential between like particles, with the relative momentum defined as $k = k_1 - k_2$, the scattering amplitude is given as

$$S(k) = -\frac{\Gamma(1 + ik/2)\Gamma(s + 1 - ik/2)}{\Gamma(1 - ik/2)\Gamma(s + 1 + ik/2)}, \quad (12)$$

where $\Gamma(\cdot)$ is the gamma function. For unlike particles, the cosh-potential are attractive, whose reflection and transmission amplitudes are given as

$$R(k) = S(k)r(k), \quad T(k) = S(k)t(k), \quad (13)$$

where

$$\begin{aligned} r(k) &= \frac{\sin \pi(s + 1)}{\sin \pi(s + 1 + ik/2)}, \\ t(k) &= \frac{\sin \pi ik/2}{\sin \pi(s + 1 + ik/2)}. \end{aligned} \quad (14)$$

Dimer bound states appear as poles of the reflection and transmission amplitudes, with binding energy $E_\tau = -(s + 1 - \tau)^2$, $\tau = 1, 2, \dots, [s + 1]$, where $[x]$ denote the largest integer less than x . The dimer can thus be described by two particles with momenta $k \pm i\kappa_\tau$, where $\kappa_\tau = s + 1 - \tau$.

For the case of $s = s'$, the system become integrable for arbitrary number of particles. No other bound states exists other than the dimer bound states mentioned above. The atom-dimer scattering amplitude between a particle with momentum k_1 and a pair of bounded particles with momenta $k_2 \pm i\kappa_\tau$ is given by

$$\exp[-i\theta_{0\tau}(k)] = S(k + i\kappa_\tau)S(k - i\kappa_\tau)t(k + i\kappa_\tau) \quad (15)$$

with $k = k_2 - k_1$. The dimer-dimer scattering amplitude $S_{\tau\tau'}(k) = \exp[-i\theta_{\tau\tau'}(k)]$ between bound atom pairs with $k_1 \pm i\kappa_\tau$ and $k_2 \pm i\kappa_{\tau'}$ are determined by the phase shift

$$\theta_{\tau\tau'}(k) = \theta_{0\tau'}(k - i\kappa_\tau) + \theta_{0\tau'}(k + i\kappa_\tau), \quad (16)$$

with $k = k_2 - k_1$. For scattering between the ground state dimers $\tau = \tau' = 1$, we have $\kappa_1 = s$, and $E_1 = -s^2$. For $s \geq 1$, the ground state dimer-dimer scattering amplitude has a simplified analytical form

$$\mathcal{S}(k) = -\frac{(s - ik/2)\Gamma(1 + ik/2)\Gamma(2s + 1 - ik/2)}{(s + ik/2)\Gamma(1 - ik/2)\Gamma(2s + 1 + ik/2)}. \quad (17)$$

Since this is the lowest scattering channel, this scattering amplitude is equivalent to the S -matrix. The closely related K -matrix is given by

$$\mathcal{K}(k) = i \frac{1 - \mathcal{S}(k)}{1 + \mathcal{S}(k)}, \quad (18)$$

and the energy-dependent dimer-dimer scattering length is given by

$$a_D(k) = \frac{1}{k\mathcal{K}(k)}. \quad (19)$$

The dimer-dimer scattering length at zero scattering energy is thus given by

$$a_D \equiv \lim_{k \rightarrow 0} a_D(k) = \frac{\gamma + s^{-1} + \psi(2s + 1)}{2}, \quad (20)$$

where $\psi(\cdot)$ is the digamma function and $\gamma = 0.577216$ is the Euler-Mascheroni constant. We will use these analytical results to benchmark our numerical calculations.

3 Results

3.1 Hyperspherical potential

To efficiently solve Eq. 8, we adopt the AHR. This involves solving the hyperangular eigenvalue problem:

$$\left[\frac{\hat{L}(\Omega)^2}{2\mu_{4b}R^2} + V(R, \Omega) \right] \Phi_\nu(R; \Omega) = U_\nu(R) \Phi_\nu(R; \Omega), \quad (21)$$

where $U_\nu(R)$ are the hyperspherical potentials, and $\Phi_\nu(\Omega; R)$ are the corresponding channel functions, which depend parametrically on hyperradius R . These functions form a truncated basis for expanding the total wave function:

$$\psi_{\nu'}^E(R, \Omega) = \sum_{\nu=1}^{N_c} F_{\nu\nu'}(R) \Phi_\nu(\Omega; R), \quad (22)$$

where ν' indexes the independent solutions and N_c is the number of channels retained in the expansion.

Before proceeding further, we note that the calculation can often be simplified by imposing permutation symmetry for identical particles. In what follows, we focus on the case of four fermions, where particles 1 and 2 are assigned $\sigma = 1$, and particles 3 and 4 are assigned $\sigma = -1$. The total wave function must be antisymmetrized using the operator

$$\mathcal{A} = 1 - \mathcal{P}_{12} - \mathcal{P}_{34} + \mathcal{P}_{12}\mathcal{P}_{34}, \quad (23)$$

where \mathcal{P}_{ij} denotes the exchange operator for particles i and j . From the expressions of the interparticle distances r_{ij} in Eq. (10), we find that \mathcal{P}_{12} has $\phi \rightarrow 2\pi - \phi$, while \mathcal{P}_{34}

maps $\phi \rightarrow \pi - \phi$, revealing the fourfold symmetry observed in the potential landscape shown in Fig. 1 (c). Since the hyperangular momentum operator takes the same form as the angular momentum operator for a single particle in three-dimensional space, the wave function can be formally expanded using spherical harmonics: $u_{\ell m_\ell}(\theta, \phi) \sim P_\ell^{m_\ell}(\cos \theta) e^{im_\ell \phi}$. Applying the antisymmetrization operator \mathcal{A} to these functions yields antisymmetrized basis functions of the form $u_{\ell k_\ell}^A(\theta, \phi) \sim P_\ell^{2k_\ell}(\cos \theta) \sin(2k_\ell \phi)$, where k_ℓ is a positive integers.

The pair-wise potential $v_{\sigma_i \sigma_j}(r)$ also exhibits certain symmetries: it is even in r , i.e., $v_{\sigma_i \sigma_j}(r) = v_{\sigma_i \sigma_j}(-r)$, and identical for like-particle pairs, i.e., $v_{11}(r) = v_{-1-1}(r)$. As a result, the full Hamiltonian is invariant under two commuting operations $\mathcal{P}_\theta : \theta \rightarrow \pi - \theta$ and $\mathcal{P}_\phi : \phi \rightarrow \pi/2 - \phi$. These symmetries allow us to define two good quantum numbers: $p_\theta = (-)^\ell$, $p_\phi = (-)^{k_\ell+1}$. Consequently, the calculation can be restricted to the reduced domain $\theta \in [0, \pi/2]$ and $\phi \in [0, \pi/4]$, with numerical basis $u_i(\theta, \phi)$ subject to the appropriate boundary conditions. We find that the ground-state dimer-dimer channel lies in the symmetry sector with $p_\theta = +1$ and $p_\phi = +1$, corresponding to even ℓ and odd k_ℓ , which implies $u_i|_{\phi=0} = 0$, $\partial_\phi u_i|_{\phi=\pi/4} = 0$, $\partial_\theta u_i|_{\theta=\pi/2} = 0$ and $u_i|_{\theta=0}$ remains finite. (Boundary conditions for other symmetry sector are summarized in Table 1.) We employ B-spline basis functions, which are piecewise polynomials with local support. This choice facilitates the implementation of boundary conditions and leads to a sparse Hamiltonian matrix that can be efficiently diagonalized using eigensolvers such as ARPACK. In practice, we typically use approximately 100 B-splines for the θ coordinate and 50 for ϕ , resulting in a sparse matrix of dimension around 5,000.

Table 1 Boundary conditions for the numerical basis functions in different symmetry sectors, characterized by p_θ and p_ϕ .

p_θ	p_ϕ	$\theta = 0$	$\theta = \pi/2$	$\phi = \pi/4$	$\phi = \pi/4$
+1	+1	Finite	$\partial_\theta u_i = 0$	$u_i = 0$	$\partial_\phi u_i = 0$
+1	-1	Finite	$\partial_\theta u_i = 0$	$u_i = 0$	$u_i = 0$
-1	+1	Finite	$u_i = 0$	$u_i = 0$	$\partial_\phi u_i = 0$
-1	-1	Finite	$u_i = 0$	$u_i = 0$	$u_i = 0$

Figure 2 and 3 present the hyperspherical potentials for $s = s' = 1.5$ across different symmetry sectors, while Figure 4 shows the hyperspherical potentials for fixed $s = 1.5$ and varying s' . A common feature among these curves is their convergence toward specific asymptotic thresholds at large hyperradii. For $s = 1.5$, the attractive interaction between unlike particles supports two dimer bound states with binding energies $E_1 = -2.25$ and $E_2 = -0.25$. As a result, the dimer-dimer thresholds appear at $E_1 + E_1 = -4.5$, $E_1 + E_2 = -2.5$, and $E_2 + E_2 = -0.5$, indicated by solid horizontal lines in the figures. The dimer-atom-atom thresholds, corresponding to single dimer binding energies E_1 and E_2 , are shown as dashed horizontal lines. The atom-atom-atom-atom threshold lies at zero energy and is indicated by dash-dotted

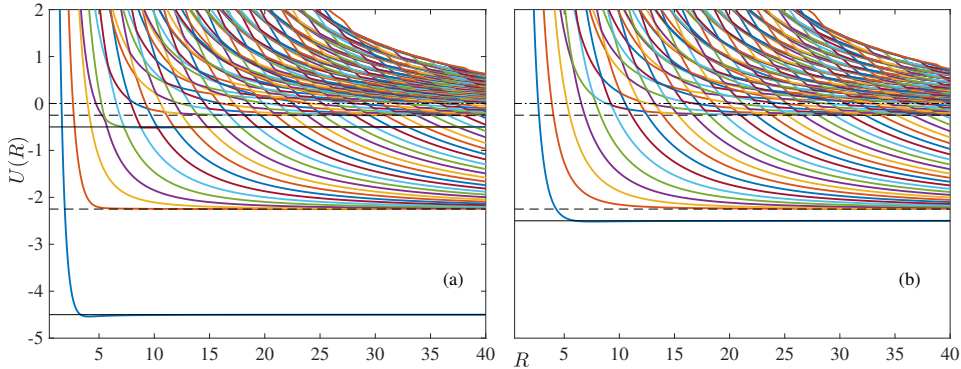


Fig. 2 Hyperspherical potential curves for $s = s' = 1.5$ in symmetry sectors: (a) $(p_\theta, p_\phi) = (+1, +1)$ and (b) $(p_\theta, p_\phi) = (+1, -1)$. Solid horizontal lines indicate dimer-dimer thresholds; dashed lines mark dimer-atom-atom thresholds; dash-dotted lines represent the atom-atom-atom-atom threshold at zero energy.

lines. An exception occurs in the second-lowest channel of Fig. 4 (b), which does not approach any of the aforementioned thresholds. This behavior arises because the reduced repulsion between like particles at $s' = 0.9$ permits the formation of trimer bound states, causing this channel to asymptotically approach a trimer-atom threshold. Additionally, many sharp avoided crossings are observed between potential curves that approach different thresholds, which may pose numerical challenges for accurate scattering calculations.

Figure 5 displays the channel functions $|\Phi_\nu(\Omega; R)|^2$ for several representative configurations. In panel (a), we show the dimer-dimer channel function corresponding to the lowest hyperspherical potential at $R = 10$ in Fig. 2 (a). Panel (b) shows the dimer-atom-atom channel function from the second-lowest channel at the same $R = 10$ in Fig. 2 (a). Panel (c) presents the atom-atom-atom-atom channel function from the 41st channel at $R = 40$ in Fig. 2 (a). Finally, panel (d) shows the trimer-atom channel function corresponding to the lowest potential at $R = 10$ in Fig. 4 (b). These channel functions reveal the spatial structure of the associated scattering configurations. The dimer-dimer channel is primarily localized in the deep blue minimum of the four-body potential landscape [see Fig. 1 (c)], while the atom-atom-atom-atom configuration occupies the broader light green plateau. The dimer-atom-atom and trimer-atom configurations are mostly concentrated along the figure-eight-shaped light blue region, highlighting the distinct geometrical signatures of different few-body scattering processes.

3.2 Scattering

With the adiabatic potential curves and diabatic corrections obtained from the channel functions, we solve the radial Schrödinger equation as a set of coupled differential equations. However, near avoided crossings, the diabatic corrections can exhibit rapid variations that lead to numerical instability. To address this challenge, we use the slow

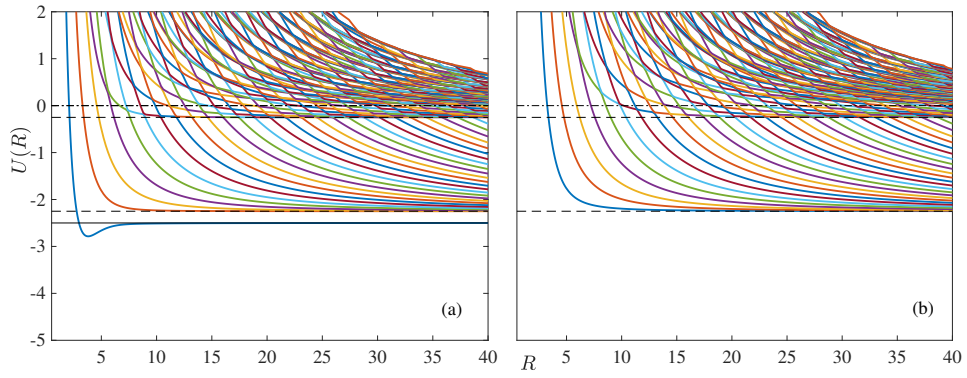


Fig. 3 Same as Fig. 2, but for symmetry sectors: (a) $(p_\theta, p_\phi) = (-1, +1)$ and (b) $(p_\theta, p_\phi) = (-1, -1)$.

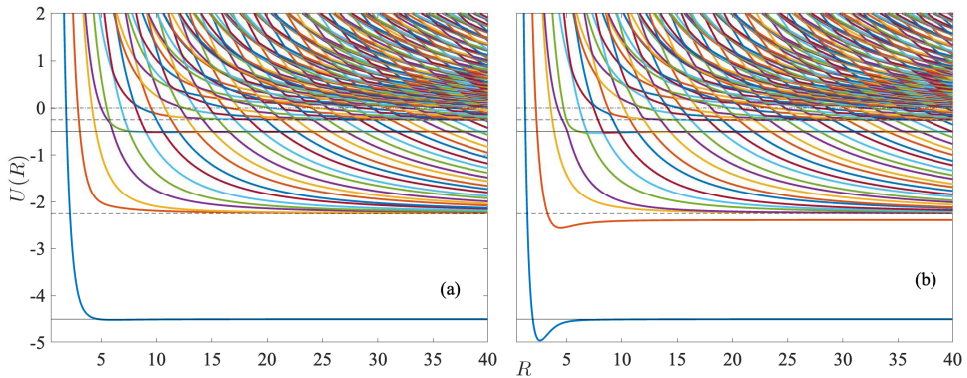


Fig. 4 Hyperspherical potential curves for $(p_\theta, p_\phi) = (+1, +1)$ and $s = 1.5$ with different s' : (a) $s' = 1.9$ and (b) $s' = 0.9$. In panel (b), the second-lowest channel approaches a trimer-atom threshold due to weakened repulsion between like particles, indicating trimer formation.

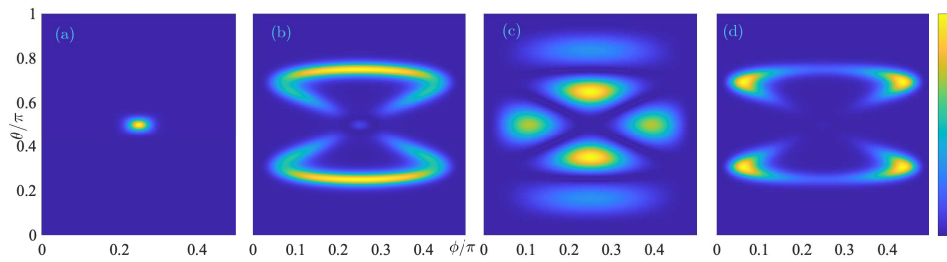


Fig. 5 Channel functions for (a) dimer-dimer channel (b) dimer-atom-atom channel (c) Four-atom channel and (d) trimer-atom channel. The color scale indicates the probability density of the wave function, shown in arbitrary units.

variable discretization (SVD) method with a radial discrete variable representation (DVR) basis $\pi_n(R)$ to expand $F_{\nu\nu'}(R)$, which gives

$$\psi_{\nu'}(R, \Omega) = \sum_{\nu, n} c_{n\nu, \nu'} \pi_n(R) \Phi_\nu(\Omega; R_n). \quad (24)$$

The DVR approximation allows integrals of the form:

$$\int_{a_1}^{a_2} \pi_i(R) H(R) \pi_j(R) dR \cong H(R_i) \delta_{ij} \quad (25)$$

for integrating smooth function $H(R)$ with quadrature method. Under this approximation, the expansion coefficients $c_{n\nu, \nu'}$ satisfy the following equation:

$$\sum_{n, \mu} T_{nn'} O_{n\nu, n'\mu} c_{n'\mu, \nu'} + [U_\nu(R_n) - E] c_{n\nu, \nu'} = 0, \quad (26)$$

with kinetic energy matrix elements:

$$T_{nn'} = \int dR \pi_n(R) \left[-\frac{1}{2\mu_{4b}} \frac{\partial^2}{\partial R^2} \right] \pi_{n'}(R) dR \quad (27)$$

and overlap matrix:

$$O_{n\nu, n'\mu} = \int d\Omega \Phi_\nu(\Omega; R_n)^* \Phi_\mu(\Omega; R_{n'}). \quad (28)$$

Once the expansion coefficients $c_{n\nu, \nu'}$ are determined, the total wave function is fully specified, allowing access to all relevant information for quantum scattering analysis.

In practice, we compute the \mathcal{R} -matrix, which serves a similar role to the inverse logarithmic derivative of the wave function in single-channel scattering problems. It is defined as

$$\mathcal{R}(R) = F(R) [\tilde{F}(R)]^{-1}, \quad (29)$$

where $F(R)$ and $\tilde{F}(R)$ denote the wave function and its derivative, respectively, evaluated at a given hyperradius R . At large distances, the physical scattering matrix \mathcal{S} (and the related reaction matrix \mathcal{K}) can be obtained by applying asymptotic boundary conditions. For dimer-dimer scattering in the lowest channel, we use:

$$\mathcal{K} = (f - f'\mathcal{R})(g - g'\mathcal{R})^{-1}, \quad (30)$$

$$\mathcal{S} = (1 + i\mathcal{K})(1 - i\mathcal{K})^{-1}, \quad (31)$$

where f and g are the regular and irregular solutions in the lowest symmetric channel:

$$f = \sqrt{\frac{2\mu_{4b}}{\pi k_H}} \cos(k_H R) \quad (32)$$

$$g = \sqrt{\frac{2\mu_{4b}}{\pi k_H}} \sin(k_H R) \quad (33)$$

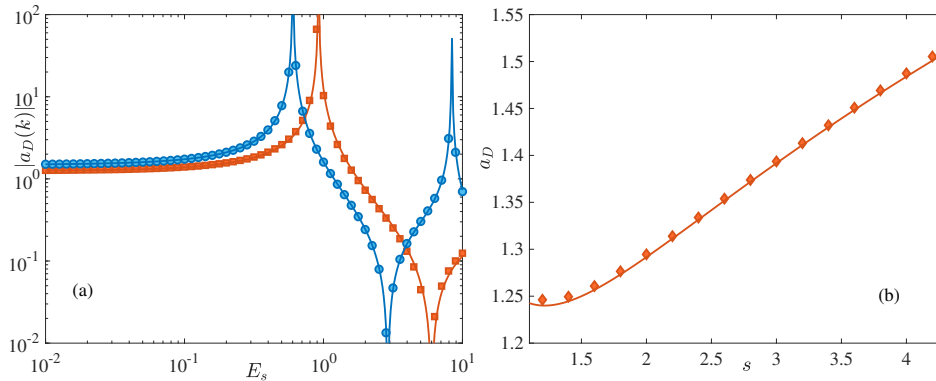


Fig. 6 Dimer–dimer scattering length between ground-state dimers for the case $s = s'$. (a) Numerical results for the energy-dependent scattering length $a_D(k)$ as a function of scattering energy E_s , shown for $s = 1.5$ (red squares) and $s = 4$ (blue circles). Solid curves represent the corresponding analytical solutions. (b) Zero-energy scattering length a_D as a function of s . Red diamonds indicate numerical results; the solid curve shows the analytical prediction.

and $k_H = \sqrt{2\mu_{4b}(E - E_{11})}$, which is the hyperradial momentum with respect to the dimer–dimer threshold energy $E_{11} = E_1 + E_1$. The scattering energy between two dimers is then $E_s = E - E_{11}$, and the dimer-dimer relative momentum is $k = \sqrt{2}k_H$. The energy-dependent scattering length is computed using Eq. (19).

Figures 6 and 7 present the computed dimer–dimer scattering lengths between ground-state dimers of the sinh-potential. In Fig. 6 (a), the energy-dependent scattering length $a_D(k)$ is shown as a function of scattering energy E_s for $s = s' = 1.5$ (red squares) and $s = s' = 4$ (blue circles). The solid curves represent the corresponding analytical solutions, with excellent agreement across all energies. Panel (b) shows the zero-energy scattering length as a function of s , numerical results (red diamonds) again match the analytical curve closely. In contrast, Fig. 7 explores the more general case where $s \neq s'$, for a fixed s and varying s' . In panel (a), the energy-dependent scattering length is plotted $s' = 0.9$ (blue circles), 1.5 (red squares), and 1.9 (purple triangles). As s' decreases, the repulsion between like particles weakens, allowing the formation of a tetramer. When the tetramer becomes bound, a resonance appears in the scattering length, which diverges as shown in panel (b). This resonance occurs near $s' \approx 0.9$, signaling the onset of tetramer binding.

4 Summary

In this work, we developed a robust and numerically accurate framework for studying four-body quantum scattering in one-dimensional systems using the adiabatic hyperspherical representation combined with the slow variable discretization method. This approach enables precise resolution of dimer-dimer scattering properties, even in the presence of sharp avoided crossings in hyperspherical potentials.

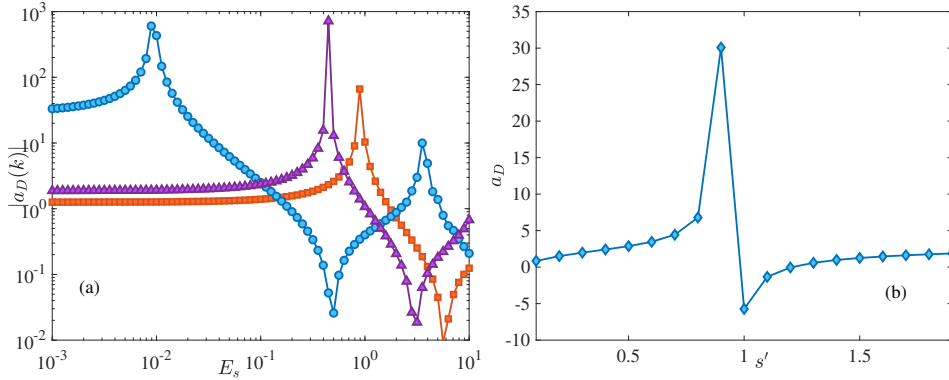


Fig. 7 Dimer–dimer scattering length between ground-state dimers for $s = 1.5$ and varying s' . Solid curves are provided as visual guides; analytical results are not available for $s \neq s'$. (a) Energy-dependent scattering length $a_D(k)$ as a function of scattering energy E_s , for $s' = 0.9$ (blue circles), 1.5 (red squares), and 1.9 (purple triangles). (b) Zero-energy scattering length a_D as a function of s' , computed numerically.

We validated our method against known analytical results for sinh-cosh model interactions, finding excellent agreement across energy scales. Extending beyond analytically tractable regimes, we explored scattering in non-integrable systems and identified a resonance in the dimer-dimer scattering length indicative of tetramer formation. These results not only affirm the accuracy of our method but also demonstrate its potential to uncover emergent few-body phenomena in low-dimensional systems.

Our findings pave the way for future investigations into more complex configurations, such as mass-imbalanced mixtures, excited-state collisions, and recombination processes. The hyperspherical approach, enhanced by SVD, offers a powerful platform for quantitatively probing universal physics in ultracold atomic gases.

Acknowledgements. J. W. acknowledges Nirav Mehta for useful discussions. This research was supported by the Australian Research Council’s (ARC) Discovery Program, Grants No. FT230100229 (J. W.), No. DP240101590 (H.H.), and No. DP240100248 (X.-J. L.).

References

- [1] Metcalf, H.J., Straten, P.: *Laser Cooling and Trapping*. Springer, New York (1999)
- [2] Dalfovo, F., Giorgini, S., Pitaevskii, L.P., Stringari, S.: Theory of bose-einstein condensation in trapped gases. *Rev. Mod. Phys.* **71**, 463–512 (1999)
- [3] Leggett, A.J.: Bose-einstein condensation in the alkali gases: Some fundamental concepts. *Rev. Mod. Phys.* **73**, 307–356 (2001)

- [4] Giorgini, S., Pitaevskii, L.P., Stringari, S.: Theory of ultracold atomic fermi gases. *Rev. Mod. Phys.* **80**, 1215–1274 (2008)
- [5] Anderson, M.H., Ensher, J.R., Matthews, M.R., Wieman, C.E., Cornell, E.A.: Observation of bose-einstein condensation in a dilute atomic vapor. *Science* **269**, 198 (1995)
- [6] DeMarco, B., Jin, D.S.: Onset of fermi degeneracy in a trapped atomic gas. *Science* **285**, 1703 (1999)
- [7] Bloch, I., Dalibard, J., Zwerger, W.: Many-body physics with ultracold gases. *Rev. Mod. Phys.* **80**, 885–964 (2008)
- [8] Chin, C., Grimm, R., Julienne, P., Tiesinga, E.: Feshbach resonances in ultracold gases. *Rev. Mod. Phys.* **82**, 1225–1286 (2010)
- [9] DeMarco, B., Jin, D.S.: Weakly bound states of three resonantly interacting particles. *Yad. Fiz.* **12**, 1080 (1970)
- [10] Kraemer, T., Mark, M., Waldburger, P., Danzl, J.G., Chin, C., Engeser, B., Lange, A.D., Pilch, K., Jaakkola, A., Nägerl, H.-C., Grimm, R.: Evidence for efimov quantum states in an ultracold gas of caesium atoms. *Nature* **440**, 315–318 (2006)
- [11] Ottenstein, T.B., Lompe, T., Kohnen, M., Wenz, A.N., Jochim, S.: Collisional stability of a three-component degenerate fermi gas. *Phys. Rev. Lett.* **101**, 203202 (2008)
- [12] Zaccanti, M., Deissler, B., D’Errico, C., Fattori, M., JonaLasinio, M., Müller, S., Roati, G., Inguscio, M., Modugno, G.: Observation of an efimov spectrum in an atomic system. *Nat. Phys.* **5**, 586–591 (2009)
- [13] Pollack, S.E., Dries, D., Hulet, R.G.: Universality in three- and four-body bound states of ultracold atoms. *Science* **326**, 1683 (2009)
- [14] Gross, N., Shotan, Z., Kokkelmans, S., Khaykovich, L.: Observation of universality in ultracold ${}^7\text{Li}$ three-body recombination. *Phys. Rev. Lett.* **103**, 163202 (2009)
- [15] Huckans, J.H., Williams, J.R., Hazlett, E.L., Stites, R.W., O’Hara, K.M.: Three-body recombination in a three-state fermi gas with widely tunable interactions. *Phys. Rev. Lett.* **102**, 165302 (2009)
- [16] Williams, J.R., Hazlett, E.L., Huckans, J.H., Stites, R.W., Zhang, Y., O’Hara, K.M.: Evidence for an excited-state efimov trimer in a three-component fermi gas. *Phys. Rev. Lett.* **103**, 130404 (2009)
- [17] Nakajima, S., Horikoshi, M., Mukaiyama, T., Naidon, P., Ueda, M.: Nonuniversal efimov atom-dimer resonances in a three-component mixture of ${}^6\text{Li}$. *Phys. Rev. Lett.* **105**, 023201 (2010)

- [18] Barontini, G., Weber, C., Rabatti, F., Catani, J., Thalhammer, G., Inguscio, M., Minardi, F.: Observation of heteronuclear atomic efimov resonances. *Phys. Rev. Lett.* **103**, 043201 (2009)
- [19] Gross, N., Shotan, Z., Kokkelmans, S., Khaykovich, L.: Nuclear-spin-independent short-range three-body physics in ultracold atoms. *Phys. Rev. Lett.* **105**, 103203 (2010)
- [20] Lompe, T., Ottenstein, T.B., Serwane, F., Viering, K., Wenz, A.N., Zürn, G., Jochim, S.: Atom-dimer scattering in a three-component fermi gas. *Phys. Rev. Lett.* **105**, 103201 (2010)
- [21] Berninger, M., Zenesini, A., Huang, B., Harm, W., Nägerl, H.-C., Ferlaino, F., Grimm, R., Julienne, P.S., Hutson, J.M.: Universality of the three-body parameter for efimov states in ultracold cesium. *Phys. Rev. Lett.* **107**, 120401 (2011)
- [22] Wild, R.J., Makotyn, P., Pino, J.M., Cornell, E.A., Jin, D.S.: Measurements of tan's contact in an atomic bose-einstein condensate. *Phys. Rev. Lett.* **108**, 145305 (2012)
- [23] Wang, J., D'Incao, J.P., Esry, B.D., Greene, C.H.: Origin of the three-body parameter universality in efimov physics. *Phys. Rev. Lett.* **108**, 263001 (2012)
- [24] Wang, Y., Wang, J., D'Incao, J.P., Greene, C.H.: Universal three-body parameter in heteronuclear atomic systems. *Phys. Rev. Lett.* **109**, 243201 (2012)
- [25] D'Incao, J.P., Wang, J., Esry, B.D., Greene, C.H.: The universality of the efimov three-body parameter. *Few-body Syst* **54**, 1523–1527 (2013)
- [26] Nishida, Y., Moroz, S., Son, D.T.: Super efimov effect of resonantly interacting fermions in two dimensions. *Phys. Rev. Lett.* **110**, 235301 (2013)
- [27] Gridnev, D.K.: Three resonating fermions in flatland: proof of the super efimov effect and the exact discrete spectrum asymptotics. *J. Phys. A* **47**, 505204 (2014)
- [28] Gao, C., Wang, J., Yu, Z.: Revealing the origin of super efimov states in the hyperspherical formalism. *Phys. Rev. A* **92**, 020504 (2015)
- [29] Nishida, Y.: Semisuper efimov effect of two-dimensional bosons at a three-body resonance. *Phys. Rev. Lett.* **118**, 230601 (2017)
- [30] Esry, B.D., Lin, C.D., Greene, C.H.: Adiabatic hyperspherical study of the helium trimer. *Phys. Rev. A* **54**, 394–401 (1996)
- [31] Suno, H., Esry, B.D., Greene, C.H., Burke, J.P.: Three-body recombination of cold helium atoms. *Phys. Rev. A* **65**, 042725 (2002)
- [32] D'Incao, J.P., Greene, C.H., Esry, B.D.: Adiabatic hyperspherical study of the

- helium trimer. *J. Phys. B.* **42**, 044016 (2009)
- [33] Wang, J., D’Incao, J.P., Greene, C.H.: Numerical study of three-body recombination for systems with many bound states. *Phys. Rev. A* **84**, 052721 (2011)
 - [34] Wang, J., D’Incao, J.P., Wang, Y., Greene, C.H.: Universal three-body recombination via resonant d -wave interactions. *Phys. Rev. A* **86**, 062511 (2012)
 - [35] Chen, Y.-H., Greene, C.H.: Efimov physics implications at p -wave fermionic unitarity. *Phys. Rev. A* **105**, 013308 (2022)
 - [36] Higgins, M.D., Greene, C.H.: Resonances and collisional properties of neutron-rich helium isotopes in the adiabatic hyperspherical representation. *Phys. Rev. C* **111**, 014001 (2025)
 - [37] Esry, B.D., Greene, C.H., Burke, J.P.: Recombination of three atoms in the ultracold limit. *Phys. Rev. Lett.* **83**, 1751–1754 (1999)
 - [38] Wang, Y., D’Incao, J.P., Greene, C.H.: Efimov effect for three interacting bosonic dipoles. *Phys. Rev. Lett.* **106**, 233201 (2011)
 - [39] Mehta, N.P., Rittenhouse, S.T., D’Incao, J.P., Greene, C.H.: Hyperspherical Approach to the Four-Body Problem. arXiv:0706.1296 (2007)
 - [40] D’Incao, J.P., Rittenhouse, S.T., Mehta, N.P., Greene, C.H.: Dimer-dimer collisions at finite energies in two-component fermi gases. *Phys. Rev. A* **79**, 030501 (2009)
 - [41] Rittenhouse, S.T., Stecher, J., D’Incao, J.P., Mehta, N.P., Greene, C.H.: The hyperspherical four-fermion problem. *J. Phys. B* **44**, 172001 (2011)
 - [42] Tolstikhin, O.I., Watanabe, S., Matsuzawa, M.: "slow" variable discretization: a novel approach for hamiltonians allowing adiabatic separation of variables. *J. Phys. B* **29**, 389 (1996)
 - [43] Wang, J.: Hyperspherical approach to quantal three-bodytheory. Phd thesis, University of Colorado, Boulder (2004)
 - [44] Sutherland, B.: Beautiful Models: 70 Years of Exactly Solved Quantum Many-Body Problems. World Scientific Publishing Company, Singapore (2004)